Comparison of the simplified GHBMC to PMHS kinematics in far-side impact

Daniel Perez-Rapela, Craig Markusic, Bryant Whitcomb, Bengt Pipkorn, Jason L. Forman, Jeff R. Crandall

Abstract Far-side impacts represent 9.5% of all automobile crashes and 8.3% of all MAIS3+ injuries. This type of event generates loads that challenge current restraint systems by setting the occupant in an inward motion. This complex motion, influenced by a number of restraint and impact parameters, often results in a loss of shoulder-to-belt contact. Existing Anthropomorphic Test Devices show limited ability to represent post-mortem human subject kinematics and sensitivity to restraint and impact parameters. Therefore, Human Body Models can play a fundamental role in understanding human response in this impact scenario. This study compares the simplified GHBMC to previously published post-mortem human subject kinematics and sensitivity to restraint and impact parameters. Results show that, in general, the simplified GHBMC captures lateral excursion in oblique impact conditions but overpredicts in purely lateral impact conditions. The simplified GHBMC shows post-mortem human subject like sensitivities to changes in ΔV and the use of pretensioner but no sensitivity to changes in impact direction. The human body model performs similarly to other previously published HBMs and obtains a "good" CORA score. However, the surrogate does not represent post-mortem human subject shoulder-to-belt interaction in all configurations.

Keywords biofidelity, corridors, far-side, GHBMC, sensitivity analysis

I. INTRODUCTION

Side impacts involving a passenger on the non-struck side of the vehicle, also known as far-side impacts, represent 9.5% of all automobile crashes and 8.3% of all MAIS3+ injuries [1]. Numerous studies point to the head and thorax as the most commonly injured body regions [1–8], with a typical intrusion profile between 3 and 4 for AIS3+ injury severity, based on the Society of Automotive Engineers (SAE) collision deformation standard [4][7]. Given that the leading cause of head injury is impact with the struck side of the vehicle [4], reducing vehicle intrusion and head excursion is crucial for injury prevention. The existing literature [9-10] shows increased head excursion in oblique cases when compared to purely lateral impacts. Complex shoulder mechanics related to loss of engagement with the shoulder belt have been hypothesised to be the causes for this counterintuitive phenomenon [10].

Current Anthropomorphic Tests Devices (ATDs) exhibit limitations in their ability to represent post-mortem human subject (PMHS) kinematics in far-side scenarios [9][11]. Limitations in shoulder motion and chest deflection undermine their ability to correctly assess the effectiveness of different restraint configurations. Moreover, improving their current level of performance may prove unfeasible with the existing ATDs and would, in any case, involve a large amount of time and investments. On the other hand, Human Body Models (HBMs) are not constrained by limitations or costs derived from physical manufacturing and therefore, they can play a fundamental role in understanding human response in these scenarios.

A number of HBM far-side biofidelity assessments can be found in the literature. The GHBMC AM50-O v4.4 (detailed GHBMC) far-side biofidelity evaluation is present in the literature [12]. However, it is difficult to evaluate the limitations of the surrogate due to changes in the friction coefficient between different loading conditions. THUMS was also evaluated in a previous study [13]. This surrogate showed satisfactory biofidelity and obtained a "good" CORrelation and Analysis (CORA) score [14].

[D]. Perez-Rapela (tel: +1-434-297-8070; e-mail: dp4db@virginia.edu) is a PhD Student, J. L. Forman is a Principal Scientist and J. R. Crandall is a Professor of Mechanical and Aerospace Engineering, all at University of Virginia, USA. C. Markusic is Chief Engineer and B. Whitcomb is Principal Engineer both at Honda R&D Americas, Inc., USA B. Pipkorn is Director of Simulation and Active Structures at Autoliv Research, Vårgårda, Sweden, and Adjunct Professor at Chalmers University of Technology in Gothenburg, Sweden.

The GHBMC M50-OS v1.8.4.1 (simplified GHBMC) allows for the evaluation of human kinematics and kinetics using a fraction of the computational time compared to the detailed version [15]. However, its biofidelity has never been assessed in far-side scenarios. The present study focuses on the comparison of the simplified GHBMC to previously-published PMHS upper body kinematics and shoulder-belt interaction in far-side impact conditions [10]. In the present study, the model was morphed to match the anthropometric measurements of different PMHSs used in the physical tests in an attempt to reduce uncertainty due to gross anthropomorphic differences. The morphed and non-morphed models were used to assess the biofidelity of the HBM kinematics and sensitivity to parameters.

II. METHODS

For the present study, 12 Finite Element (FE) LS-Dyna simulations replicating six existing PMHS test configurations [10] were conducted using the simplified GHBMC v1.8.3.1. The selected configurations (TABLE I) include variations in pulse intensity (34 km/h and 14 g, 16 km/h and 6.6 g), impact direction (oblique 60°, lateral 90°), D-ring location (forward, intermediate, back), pretensioner usage (yes, no) and additional pelvic restraint (yes, no).

TABLE I
IMPACT CONFIGURATIONS

Conf. #	ΔV (km/h)	Impact Direction	D-Ring Position	Pretensioner	Pelvic restraint
1	16	Oblique	Intermediate	No	No
2	16	Oblique	Intermediate	Yes	No
3	34	Oblique	Intermediate	Yes	No
4	16	Oblique	Back	Yes	Yes
5	16	Lateral	Forward	Yes	No
6	34	Lateral	Intermediate	Yes	No

The FE model of the physical buck was created based on the original CAD parts (Fig. 1). Model parts were defined as rigid, when possible, for time efficiency. The coordinate system for the kinematic evaluation was defined at the centre of the upper surface of the seat pan with its axis following the SAE J670 standard [16]. The seatbelt retractor parameters were reversed engineered based on quasi-static tests in combination with information derived from previously published dummy tests [11]. The friction between the different model components was set based on quasi-static friction tests. Friction between the HBM and the seatbelt webbing was set to 0.5.

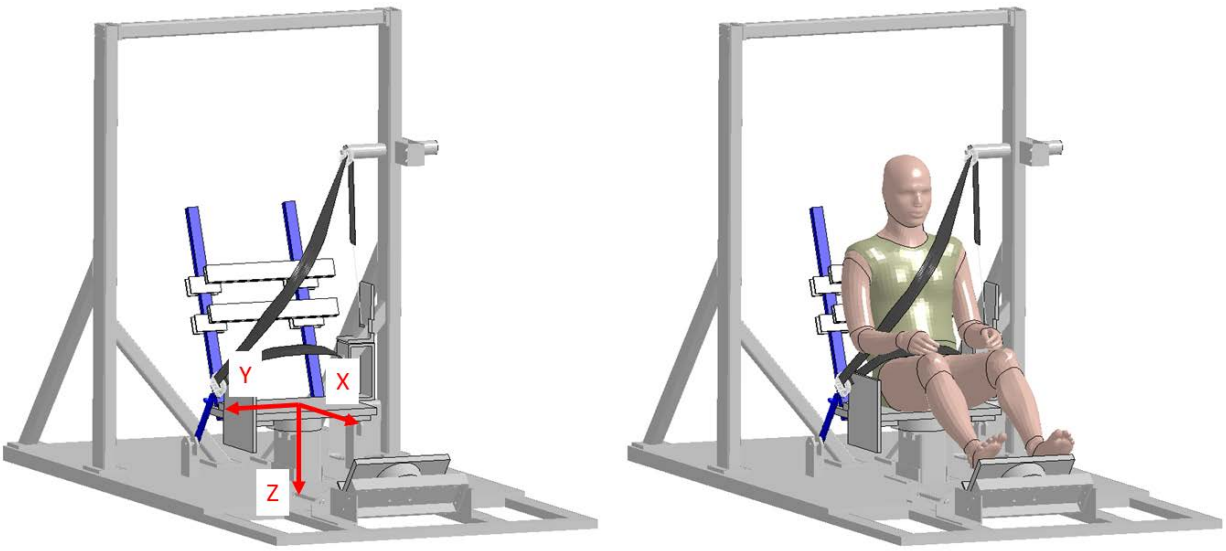

Fig. 1. Simulation model for the buck and restraint system. Grey: rigid; blue: deformable.

Two different strategies were followed regarding the use of the HBM. In the first strategy, the 6 configurations were replicated with the simplified GHBMC matching the average PSIS location and upper body angle of the PMHS used in each configuration. In the second strategy, the HBM was morphed to represent the anthropometry of an individual PMHS used in the configuration of interest (TABLE II). In this second strategy, the HBM was positioned to match the seatbelt routing and the PSIS, pelvis pitch, T1, acromions and head location of the PMHS test. The average positioning error was 10 mm for PSIS and T1, 15 mm for head, 18 mm for acromions and 3.5 degrees for pelvis pitch. The PMHS anthropometric measurements were obtained using CT-scans, 3D tracking information and test images. Morphed and non-morphed HBMs were settled by gravity and the resulting stress and strain information was carried to the final simulation.

The morphing process was automated with a MatLab-PIPER script that calculates control and target points and runs the Kriging method in a patched-compilation of PIPER 1.0.2. This script morphs the model in two steps (Fig. 2). In a first step, the model is morphed to match anthropometric measurements that involve hard and soft tissue morphing, i.e., gross shape. In a second step, the bones are rigidised, and the soft tissue is morphed to match anthropometric measurements that do not necessarily affect hard tissue, e.g., abdominal circumference. Once the geometric morphing was concluded, the PMHS weight was matched by scaling the density of the HBM soft tissue. The resulting morphed models have an error < 1% with respect to the target values in TABLE II. However, since there are multiple sources of variability that cannot be accounted for, e.g., spine curvature or shoulder shape, this morphing approach does not attempt to generate PMHS-specific models but to remove part of the uncertainty due to gross anthropomorphic differences that may confound the effect of other surrogate characteristics, e.g., soft tissue stiffness.

TABLE II
MORPHING TARGETS (IN MM EXCEPT NOTED) AND AVERAGE VALUES FOR ALL PMHS USED IN THE STUDY

Anthropometric Measurement	Information Source	PMHS# 602 Conf. 1,2,3	PMHS# 587 Conf. 4	PMHS# 551 Conf. 5	PMHS# 559 Conf. 6	All PMHS Mean (S.D.)
Weight [kg]	Manual Measurement	79	91	83	73	82 (6)
PSIS to T1 distance	3D tracking	468	480	499	492	477 (20)
T1 to Head distance	3D tracking	136	156	145	168	153 (9)
*Biacromial breadth**	3D tracking	310	257	293	297	292 (21)
*Chest depth***	3D tracking	106	117	141	91	117 (16)
*Chest breadth**	Manual Measurement	334	351	355	298	328 (29)
*Waist depth***	3D tracking	244	279	259	250	247 (25)
*Waist breadth**	Images	324	348	351	284	311 (35)
Pelvis height	CT-Scan	197	215	199	200	202 (8)
Pelvis depth	CT-Scan	137	148	140	131	139 (6)
Pelvis breadth	CT-Scan	264	277	269	270	264 (10)
*Thigh link**	3D tracking	398	430	368	403	405 (25) †
*Thigh circ.**	Manual Measurement	570	618	578	528	490 (84) †
*Lower Thigh circ.**	Manual Measurement	392	488	350	392	405 (46) †
*Calf link**	3D tracking	389	410	396	412	403 (23)
*Acromion-Radiale length**	3D tracking	317	349	318	337	319 (12)
*Elbow-Wrist length**	3D tracking	225	267	246	253	254 (17)
*Biceps circ.**	Manual Measurement	306	311	312	266	285 (30) †

† Measured in the supine position

* Measured following guidelines defined in [17]

** Perpendicular distance from external surface and a plane located parallel to Y passing through PSIS and T1

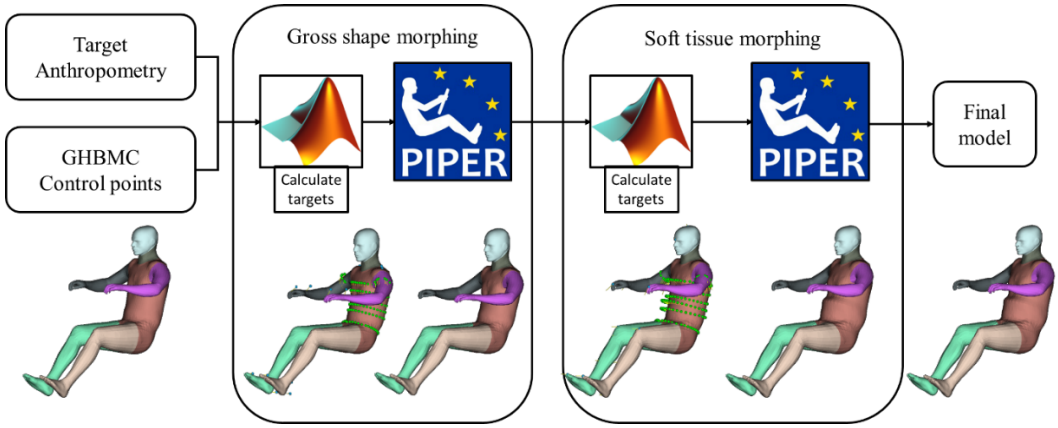

Fig. 2. MatLab-PIPER morphing script flow-chart.

Once the simulations were conducted, the GHBMC upper body kinematics and seatbelt engagement were compared to previously published PMHS corridors and test images [10-11]. These corridors represent the average ± 1 standard deviation of a small (n≤3) non-scaled PMHS test sample. Since these corridors represent only a small portion of the population and the morphing process could not account for multiple sources of variability, these corridors were used to evaluate not only the non-morphed models but also the morphed models. These evaluations focused on assessing upper body kinematics and seatbelt engagement using the CORA method [18]. This method assigns a correlation score between the HBMs and the PMHS responses by applying two methods: the corridor method and the cross-correlation method. The corridor method analyses the fitting of the response into the PMHS corridor. The cross-correlation method consists of a comparison of the phase, shape and area below the HBM and PMHS responses. The final CORA score is calculated as a weighted average of the two methods:

$$CORA_{Score} = 0.5 \cdot Score_{corridor} + 0.5 \cdot (0.5 \cdot Score_{shape} + 0.25 \cdot Score_{phase} + 0.25 \cdot Score_{area}) \quad (1)$$

Additionally, a linear regression was conducted to assess the HBM's ability to represent PMHS lateral head excursion sensitivity to changes in impact parameters.

III. RESULTS

Upper Body Motion and Seatbelt Engagement

Since the HBM neck introduces passive musculature, this section focuses on T1 instead of head excursion. Moreover, since the shoulder lateral motion is highly correlated to that of T1, only the fore-aft left shoulder motion was evaluated in this section. More kinematic results and images can be found in Appendix A and B.

Oblique impact direction

T1 motion shows good agreement with PMHS corridors in the oblique impact direction (Fig. 3). The morphed model shows better CORA scores than the non-morphed model for all loading conditions except for Configuration 1 where both models perform virtually the same.

The model shows PMHS-like shoulder motion in the low-speed cases without additional pelvic restraint (Conf. 1 and 2). However, it tends to show a lack of initial forward shoulder motion, particularly in the high-speed case (Conf. 3). This translates to differences in shoulder belt engagement (Fig. 4-right).

The HBM replicates the shoulder belt engagement of at least one of the PMHS used in each configuration with the exception of the high-speed case (Appendix B, Figure B1 to B4). In this loading condition, the abdomen of the PMHS expands forward preventing the shoulder belt from sliding (Fig. 7). This leads to a change in body kinematics that the HBM is not able to represent.

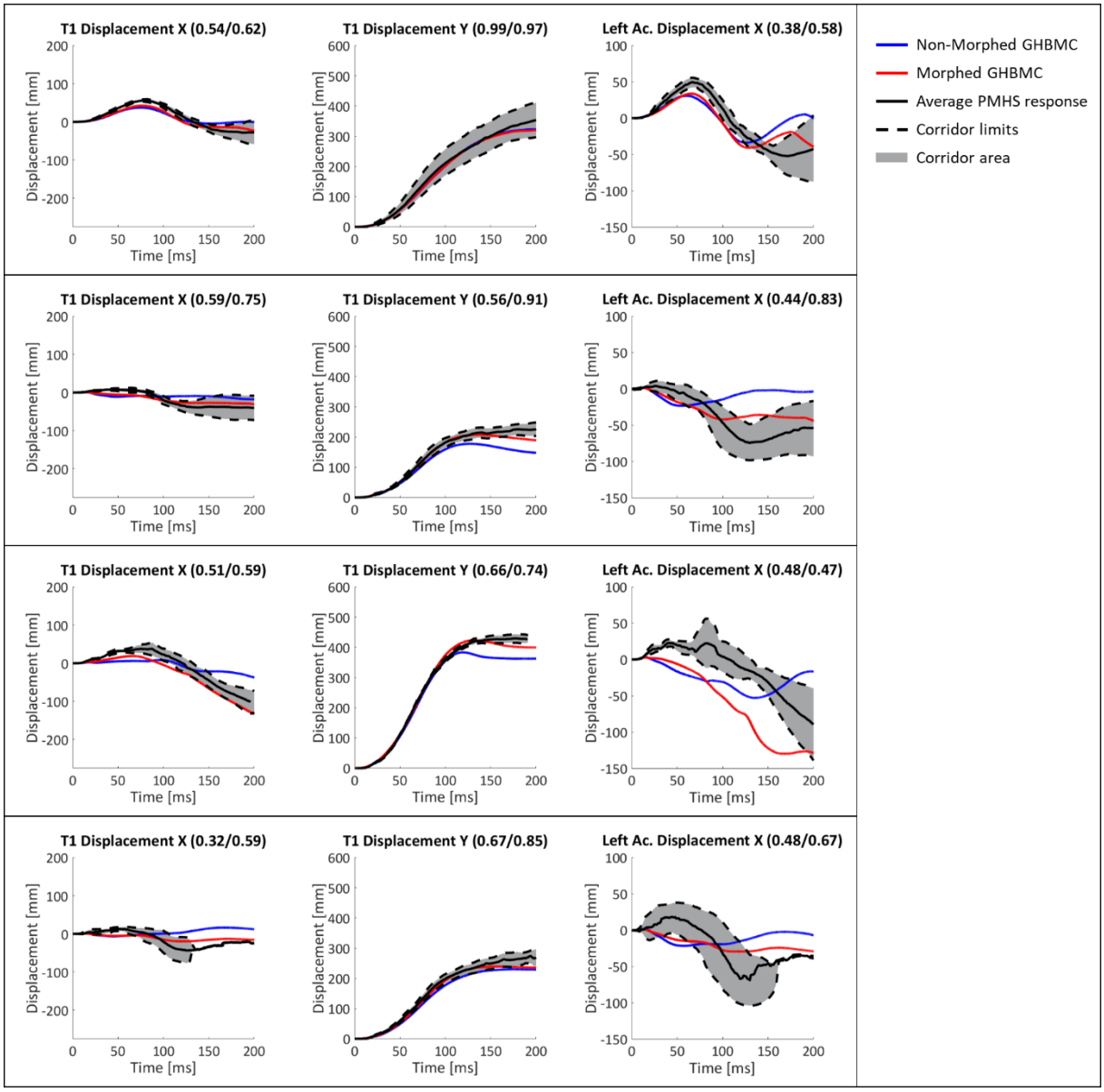

Fig. 3. GHBMC upper body kinematics in oblique impact directions: Configuration 1 to 4 (up to down). CORA score of non-morphed and morphed models in parenthesis.

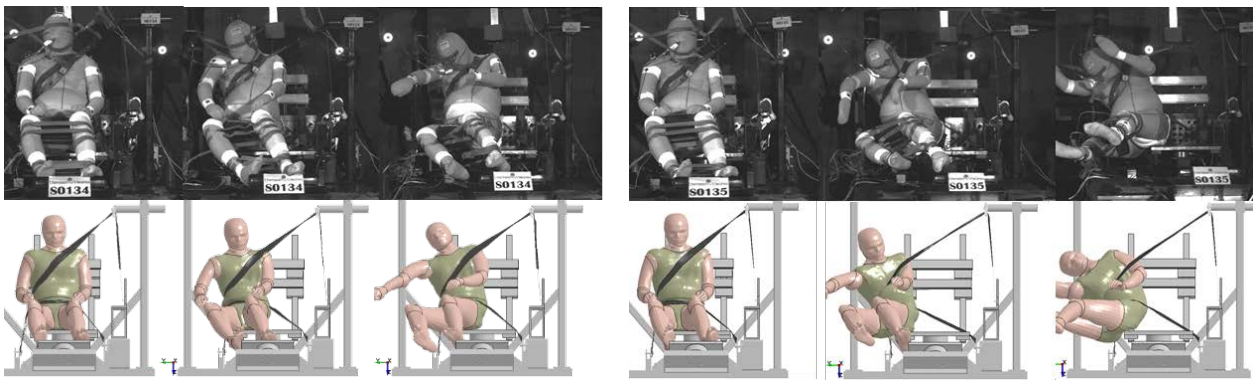

Fig. 4. Morphed GHBMC and PMHS kinematics at 50, 100 and 150ms in Configuration 2 (left) and 3 (right).

Lateral impact direction

The GHBMC shows PMHS-like fore-aft upper body motion in purely lateral directions. However, although the shoulder belt contacts the HBM laterally in a region similar to the PMHS, the HBM overestimates PMHS lateral excursion (Fig. 5, Fig. 6, Appendix B, Figure B5 and B6). Morphing the model improves fore-aft motion but it leads to slightly worse results in lateral excursion for the high-speed case.

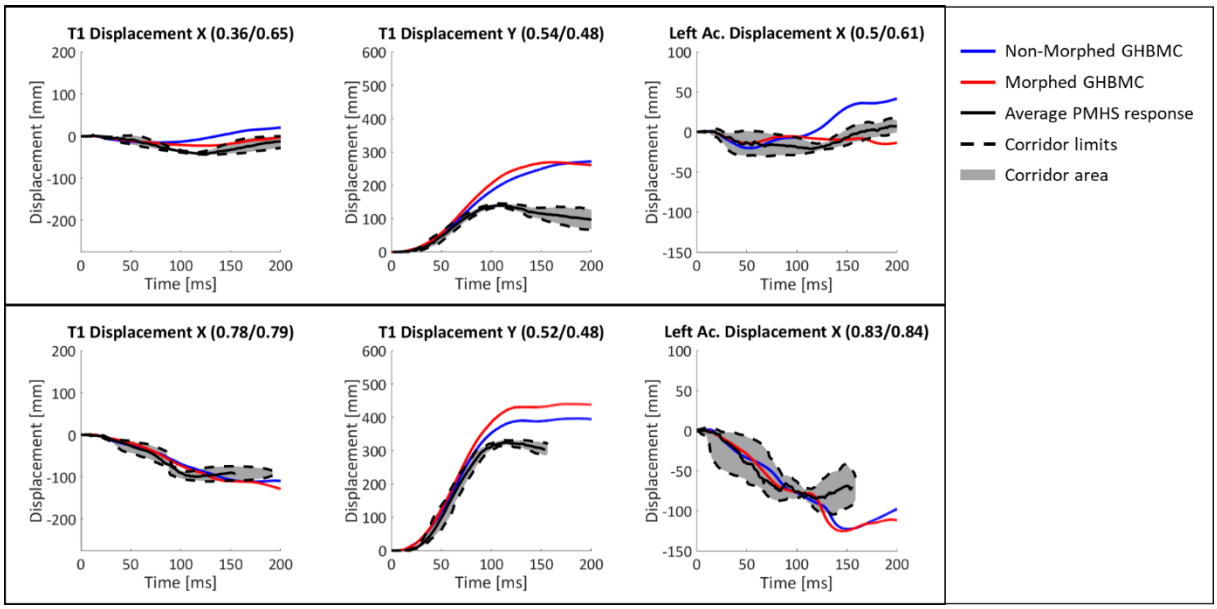

Fig. 5. GHBMC upper body kinematics in purely lateral impact directions: Configuration 5 (up) and 6 (down). CORA score of non-morphed and morphed models in parenthesis.

Fig. 6. Morphed GHBMC and PMHS kinematics at 50, 100 and 150ms in Configuration 5 (left) and 6 (right).

CORA scores

The CORA scores associated with the different upper body regions are summarized in TABLE III. The non-morphed and morphed models show an overall “fair” and “good” score based on ISO rating [14]. The shoulder obtains high scores, particularly in the morphed model, averaging 0.67 in the morphed model and 0.52 in the non-morphed model.

The morphed model shows equal or improved CORA scores compared to the non-morphed model in all body regions with the exception of T1 lateral excursion in purely lateral impact direction cases. The shoulder is the body region that shows the largest improvement from morphing, from 0.45 to 0.64 in oblique impacts. The loading condition that shows the largest morphing-related improvement is configuration 2.

TABLE III
CORA SCORES (NON-MORPHED/MORPHED)

Conf. #	T1		Shoulder	Average per configuration
	Long.	Lat.	Long.	
1	0.54 / 0.62	0.99 / 0.97	0.38 / 0.58	0.64 / 0.73
2	0.59 / 0.75	0.56 / 0.91	0.44 / 0.83	**0.53 / 0.83**
3	0.51 / 0.59	0.66 / 0.74	0.48 / 0.47	0.55 / 0.6
4	0.32 / 0.59	0.67 / 0.85	0.48 / 0.67	0.49 / 0.7
Average per body motion PDOF = 60°	0.49 / 0.64	**0.72 / 0.87**	**0.45 / 0.64**	0.55 / 0.71
5	0.36 / 0.65	0.54 / 0.48	0.5 / 0.61	0.47 / 0.58
6	0.78 / 0.79	0.52 / 0.48	0.83 / 0.84	0.71 / 0.7
Average per body motion PDOF = 90°	0.57 / 0.72	**0.53 / 0.48**	0.66 / 0.72	0.59 / 0.64
Average per body motion	0.52 / 0.67	0.66 / 0.74	**0.52 / 0.67**	**0.56 / 0.69**

Sensitivity to parameters

Morphed and non-morphed models show similar sensitivity to impact parameters (TABLE IV). Changes in impact pulse lead to an approximate average increase of 4.8 mm/g in lateral head excursion. The model shows shorter lateral head excursion in oblique impacts compared to purely lateral events. Pretensioner use reduces lateral head excursion in 144 mm and 196 mm respectively for the morphed and non-morphed GHBMC.

TABLE IV
HEAD LATERAL DISPLACEMENT (MM)

Predictor		Coefficient Non-Morphed	Coefficient Morphed
Constant		276.5	144.7
Pulse (g)		**34.7**	**36.1**
Impact direction (deg.)		**0.64**	**1.78**
*D-Ring**	*forward*	36.0	-28.9
	intermediate	-96.1	-73.3
*Pretensioner***		**-196.0**	**-143.9**

*Discrete predictor. **Dichotomous variable: No=0, Yes=1

IV. DISCUSSION

Representing occupant upper body kinematics and shoulder belt engagement is key to understanding and developing effective restraints for far-side scenarios. The simplified GHBMC shows PMHS-like kinematic response in the low-speed oblique impact conditions. T1 motion is correctly captured in all oblique cases. However, shoulder belt engagement differs from PMHS responses in the purely lateral cases and the oblique high-speed case. This leads to an overestimation of lateral excursion in purely lateral impact scenarios.

There are multiple factors that can potentially contribute to these differences in shoulder belt engagement. Results of the morphed model shows that external anthropometry accounts for some of the differences in upper body motion and seatbelt engagement. However, these factors do not account for all the kinematic differences between the HBM and PMHS.

Soft tissue deformation and weight distribution seem to have an effect on upper body kinematics and shoulder belt engagement. Fig. 7 and those in Appendix B show how the abdomen of some PMHSs tends to expand forward after impact. This phenomenon has two effects. First, it generates an inertial load on the lower portion of the upper body that may influence whole body kinematics and second, it prevents the shoulder belt from sliding off the upper body. Limitations in current material definitions and element formulations for the abdominal area prevent the HBM from capturing this phenomenon.

Fig. 7. Abdominal expansion in PMHS test at 0 ms., 50 ms., and 75 ms.

Representing kinematics in purely lateral impacts and sensitivity to changes in impact direction seems to be particularly challenging. This issue is consistent with previous ATD and HBM biofidelity studies based on these PMHS tests [11–13]. This may be an indication that either there are consistent differences between the PMHS used in this loading condition and the average HBM, e.g., weight distribution, or that current modelling techniques cannot represent phenomena associated with shoulder belt retention, e.g., soft tissue expansion.

The HBM shows good CORA scores, given the relatively small PMHS samples used to construct the corridors. These scores are comparable to previously evaluated HBMs [12-13]. Shoulder motion shows the largest improvement after morphing the model. This indicates that the differences in shoulder motion may be not directly or solely attributable to the shoulder area but to overall body shape and deformation.

V. CONCLUSIONS

The simplified GHBMC shows good agreement with PMHS kinematics. The model performs better in oblique impact conditions.

The discrepancies observed in the study are consistent with those found in previous HBM studies. It is unclear if these discrepancies are due to limitations in the material models, meshing methodologies or PMHS sample size.

VI. ACKNOWLEDGEMENTS

Tomas Janak provided expedited help with PIPER-scripting. Tim Gillispie reviewed the grammar in this manuscript.

VII. REFERENCES

[1] Bahouth GT, Murakhovskiy D, Digges KH, Rist H, Wiik R. Opportunities for reducing far-side casualties. *24th Int. Tech. Conf. Enhanced Safety Veh. (ESV)*, 2015.

[2] Mackay GM, Hill J, Parkin S, Munns JAR. Restrained occupants on the nonstruck side in lateral collisions. *Accident Analysis & Prevention*, 1993, 25(2):147–152.

[3] Frampton R, Welsh R, Thomas P, Fay P. The Importance of Non-struck Side Occupants in Side Collisions. *Journal of Crash Prevention and Injury Control*, 2000, 2(2):151–163.

[4] Gabler HC, Fitzharris M, et al. Far side impact injury risk for belted occupants in Australia and the United States. *Proceedings of the nineteenth international conference on enhanced safety of vehicles*, 2005.

[5] Ryb GE, Dischinger PC, et al. Expected Differences and Unexpected Commonalities in Mortality, Injury Severity, and Injury Patterns Between Near Versus Far Occupants of Side Impact Crashes. *The Journal of Trauma: Injury, Infection, and Critical Care*, 2009, 66(2):499–503.

[6] Viano DC, Parenteau CS. Severe Injury to Near- and Far-Seated Occupants in Side Impacts by Crash Severity and Belt Use. *Traffic Injury Prevention*, 2010, 11(1):69–78.

[7] Yoganandan N, Arun MWJ, et al. Crash Characteristics and Injury Patterns of Restrained Front Seat Occupants in Far-side Impacts. *Traffic Injury Prevention*, 2014, 15(sup1):S27–S34.

[8] Brumbelow ML, Mueller BC, Arbelaez RA. Occurrence of Serious Injury in Real-World Side Impacts of Vehicles with Good Side-Impact Protection Ratings. *Traffic Injury Prevention*, 2015, 16(sup1):S125–S132.

[9] Pintar FA, Yoganandan N, et al. Comparison of PMHS, WorldSID, and THOR-NT responses in simulated far side impact. *Stapp car crash journal*, 2007, 51:313.

[10] Forman JL, Lopez-Valdes F, et al. Occupant kinematics and shoulder belt retention in far-side lateral and oblique collisions: a parametric study. *SAE Technical Paper*, 2013.

[11] Perez-Rapela D, Markusic C, et al. Comparison of WorldSID to PMHS kinematics in far-side impact. *IRCOBI Conference Proceedings*, 2018, Athens, Greece.

[12] Katagiri M, Zhao J, Kerrigan J, Kent R, Forman J. Comparison of Whole-Body Kinematic Behaviour of the GHBMC Occupant Model to PMHS in Far-Side Sled Tests. *IRCOBI Conference Proceedings*, 2016, Malaga, Spain.

[13] Pipkorn B, Larsson K, et al. Occupant Protection in Far-Side Impacts. *IRCOBI Conference Proceedings*, 2018, Athens, Greece.

[14] ISO/TR- 9790, Road vehicles-anthropomorphic side impact dummy-Lateral impact response requirements to assess the biofidelity of the dummy. *International Organization for Standardization*, 1999.

[15] Schwartz D, Guleyupoglu B, Koya B, Stitzel JD, Gayzik FS. Development of a Computationally Efficient Full Human Body Finite Element Model. *Traffic Injury Prevention*, 2015, 16(sup1):S49–S56.

[16] Society of Automotive Engineers, Vehicle Dynamics Terminology. 2008.

[17] Gordon CC, Blackwell CL, et al. 2012 Anthropometric survey of US Army personnel: Methods and summary statistics. Army Natick Soldier Research Development and Engineering Center, MA, 2014.

[18] Gehre C, Gades H, Wernicke P. Objective Rating of Signals Using Test and Simulation Responses. *Proceedings: International Technical Conference on the Enhanced Safety of Vehicles*, 2009.

VIII. APPENDIX A

This appendix contains the simplified GHBMC (red) upper body motion and seatbelt forces and the corresponding PMHS corridors for each test configuration

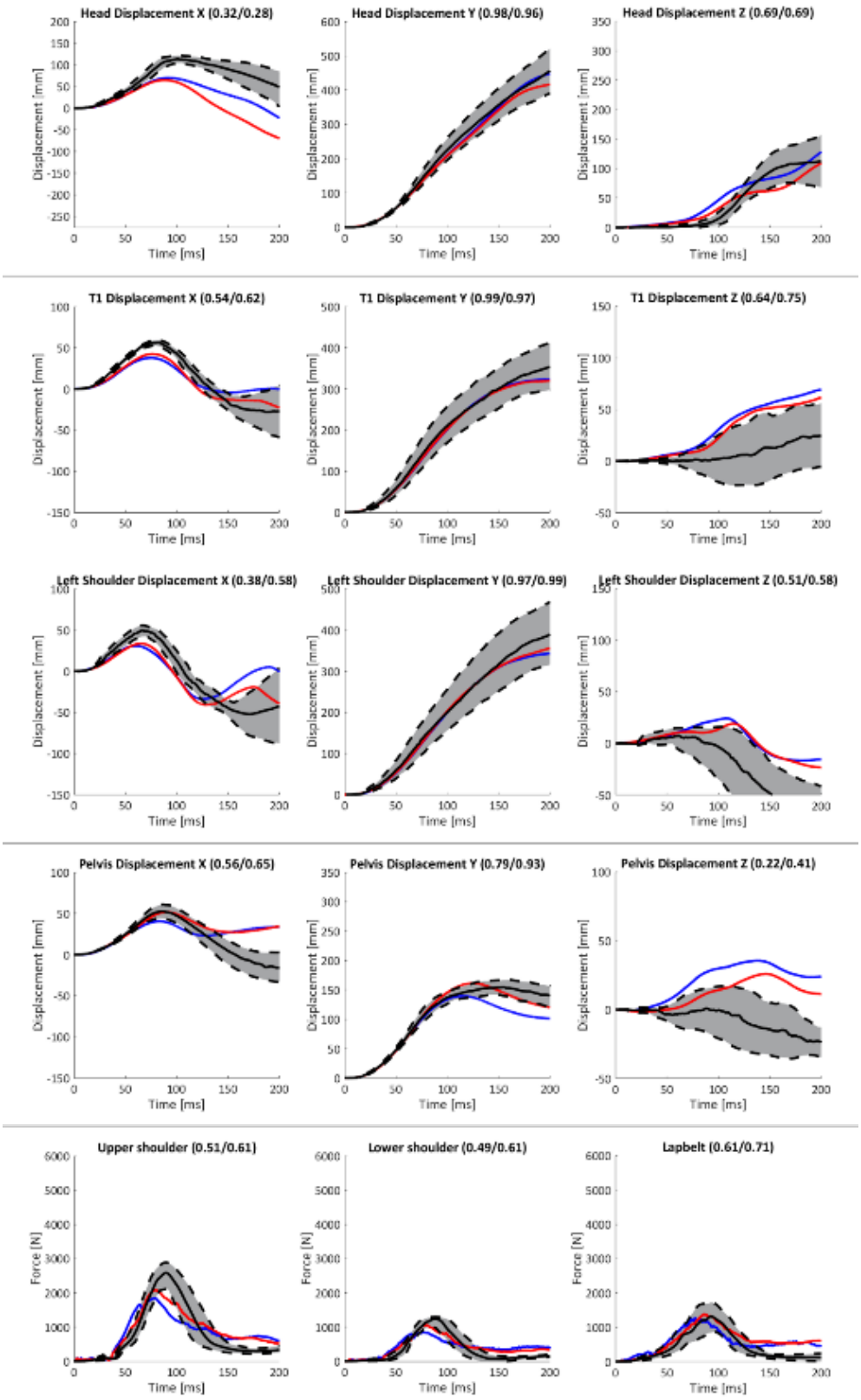

Fig. A1. Simplified GHBMC and PMHS response in configuration 1
CORA Scores in parenthesis (non-morphed/morphed).

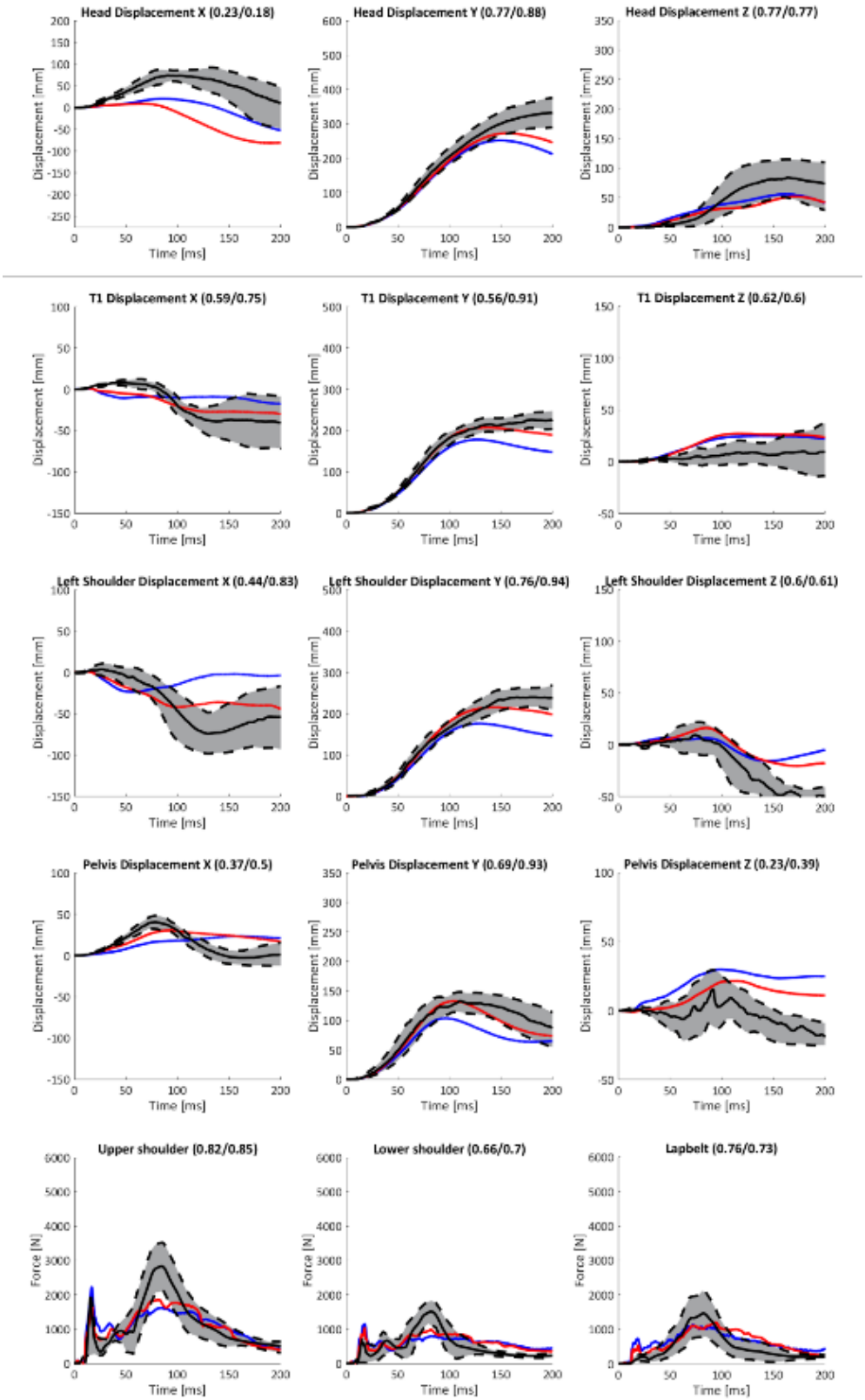

Fig. A2. Simplified GHBMC and PMHS response in Configuration 2
CORA Scores in parenthesis (non-morphed/morphed).

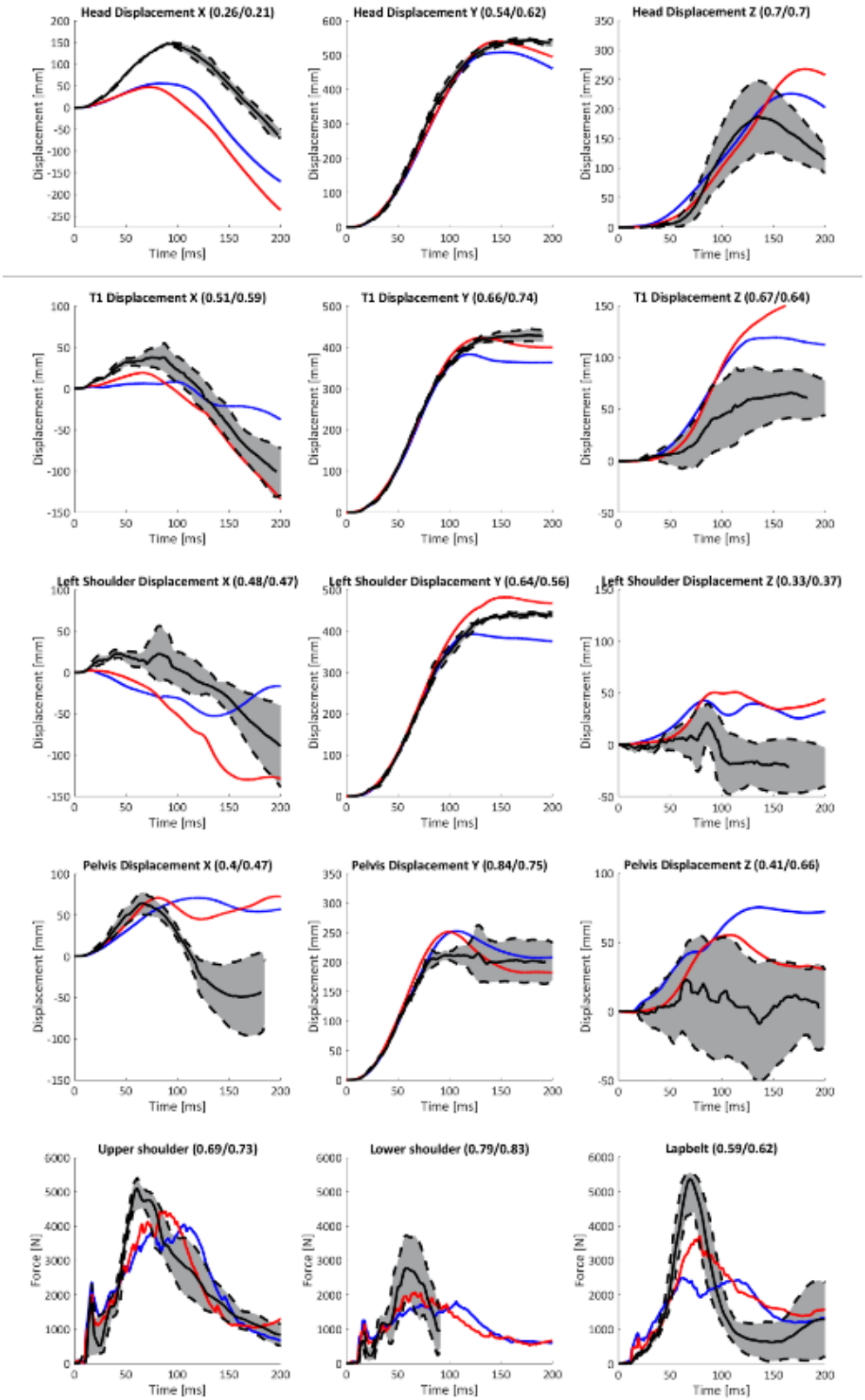

Fig. A3. Simplified GHBMC and PMHS response in Configuration 3
CORA Scores in parenthesis (non-morphed/morphed).

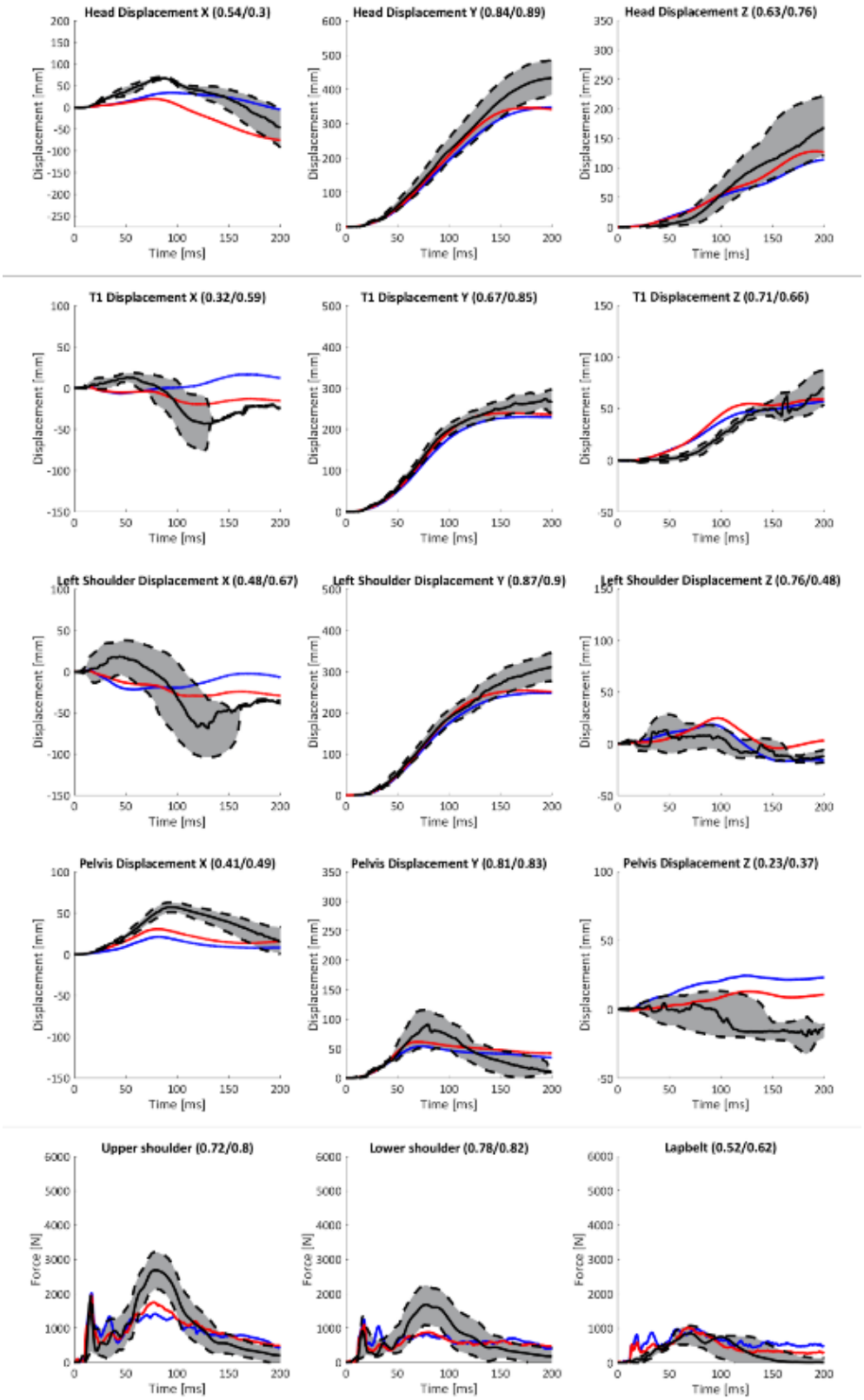

Fig. A4. Simplified GHBMC and PMHS response in Configuration 4
CORA Scores in parenthesis (non-morphed/morphed).

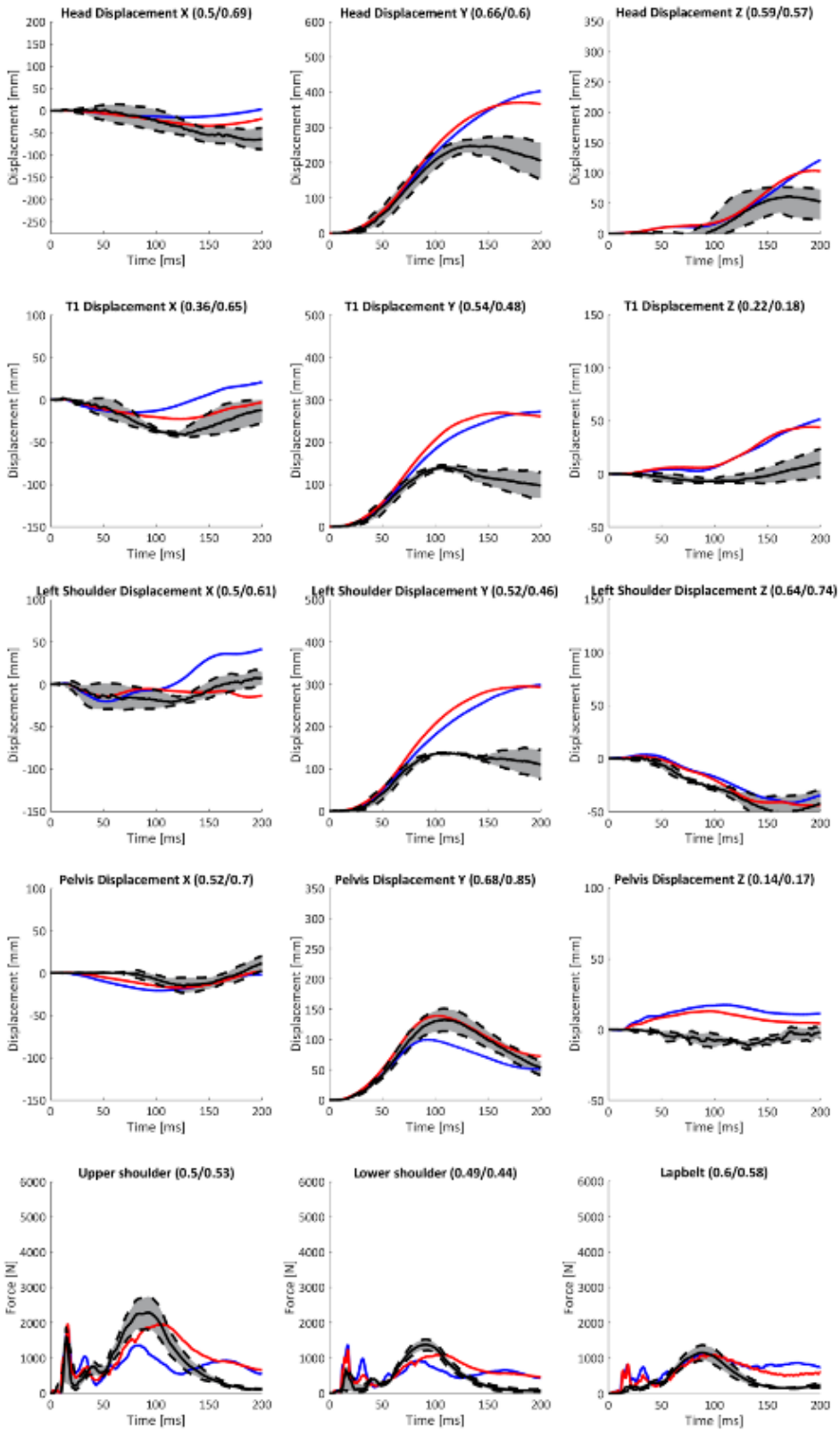

Fig. A5. Simplified GHBMC and PMHS response in Configuration 5
CORA Scores in parenthesis (non-morphed/morphed).

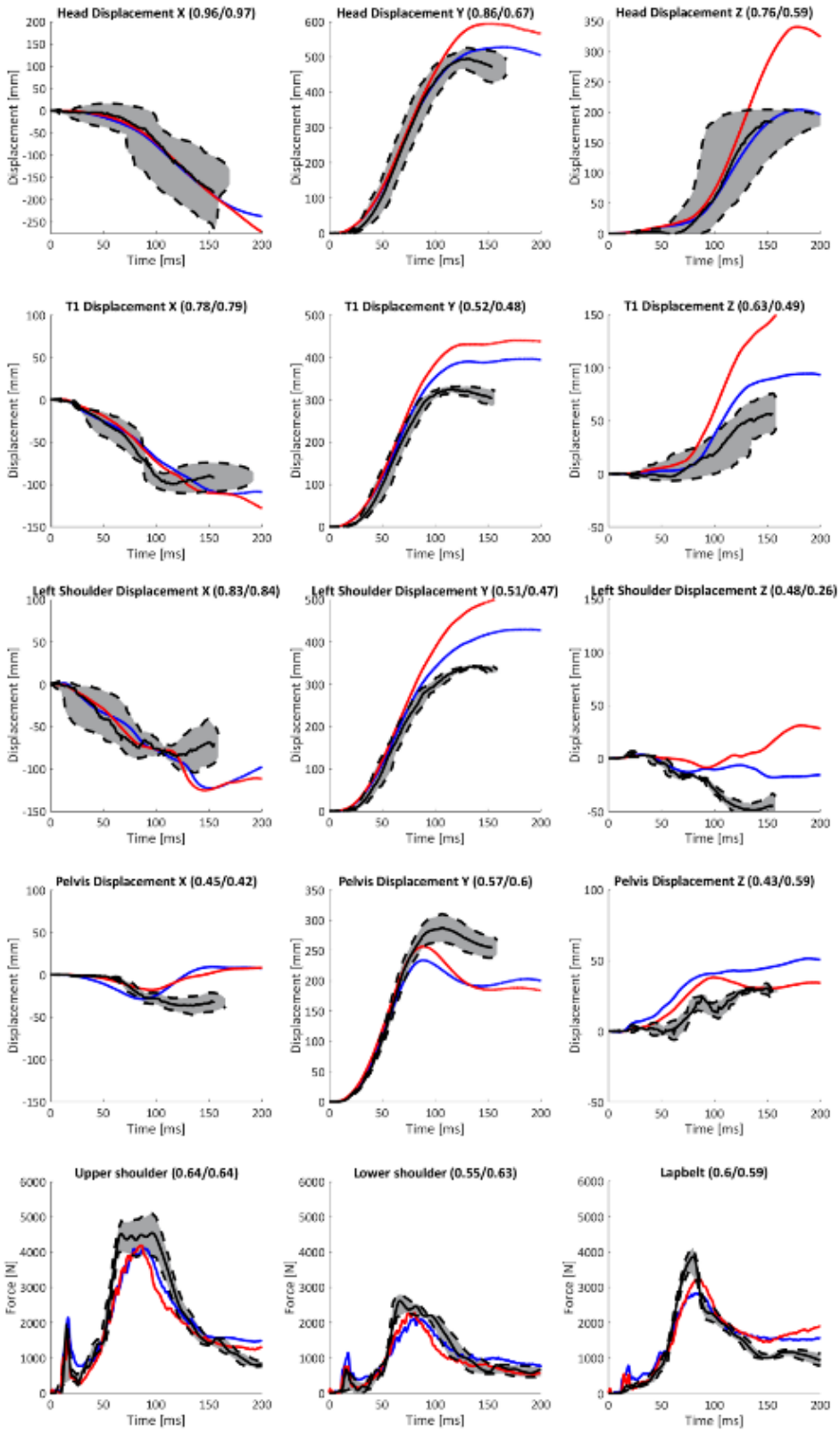

Fig. A6. Simplified GHBMC and PMHS response in Configuration 6
CORA Scores in parenthesis (non-morphed/morphed).

IX. APPENDIX B

This appendix contains the images extracted from the simulations and PMHS tests for each test configuration. The morphed HBM and the PMHS used in its morphing are highlighted in red.

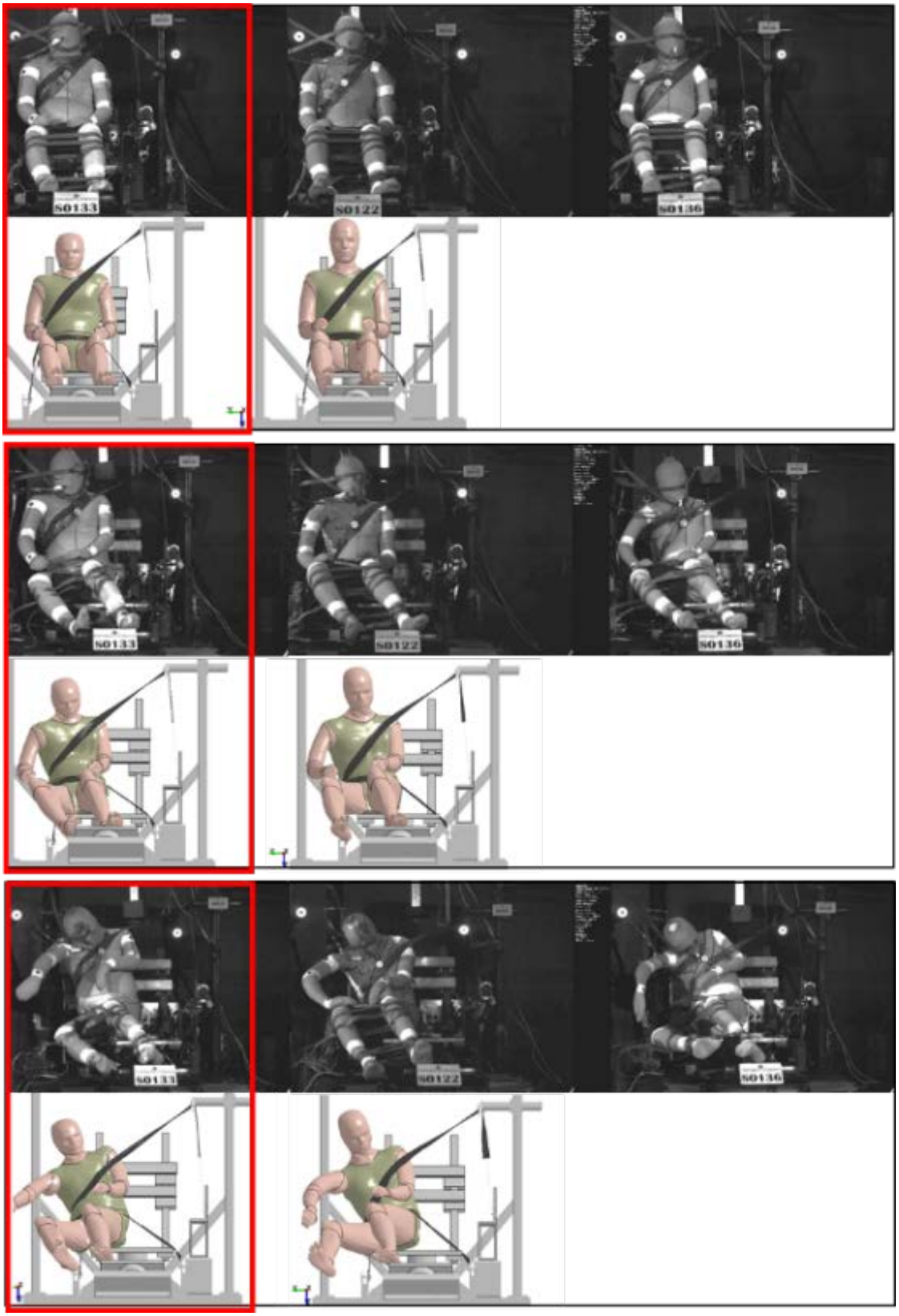

Fig. B1. Simplified GHBMC and PMHS response in Configuration 1 at 50 ms (up), 100 ms (centre) and 150 ms (down).

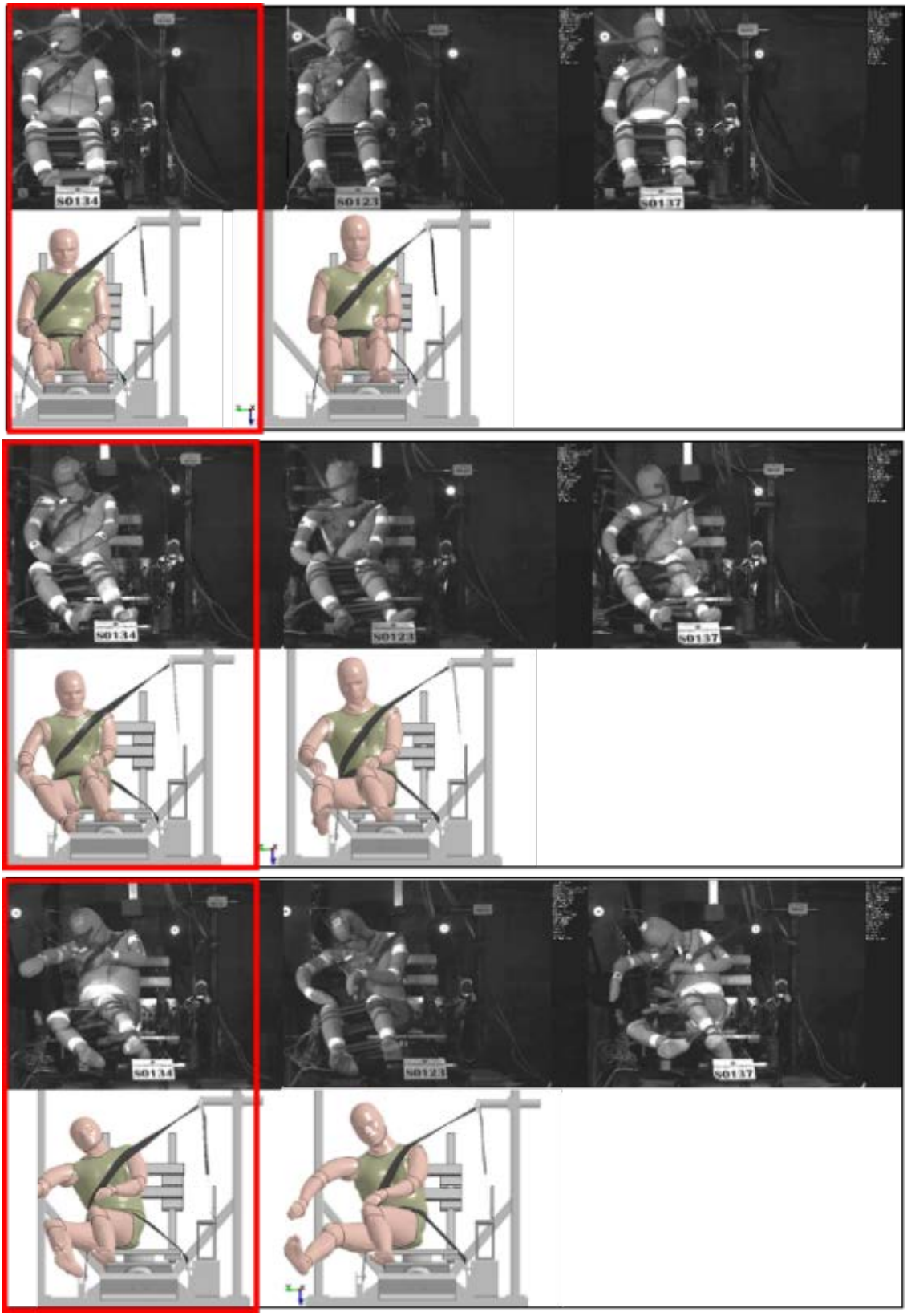

Fig. B2. Simplified GHBMC and PMHS response in Configuration 2 at 50 ms (up), 100 ms (centre) and 150 ms (down).

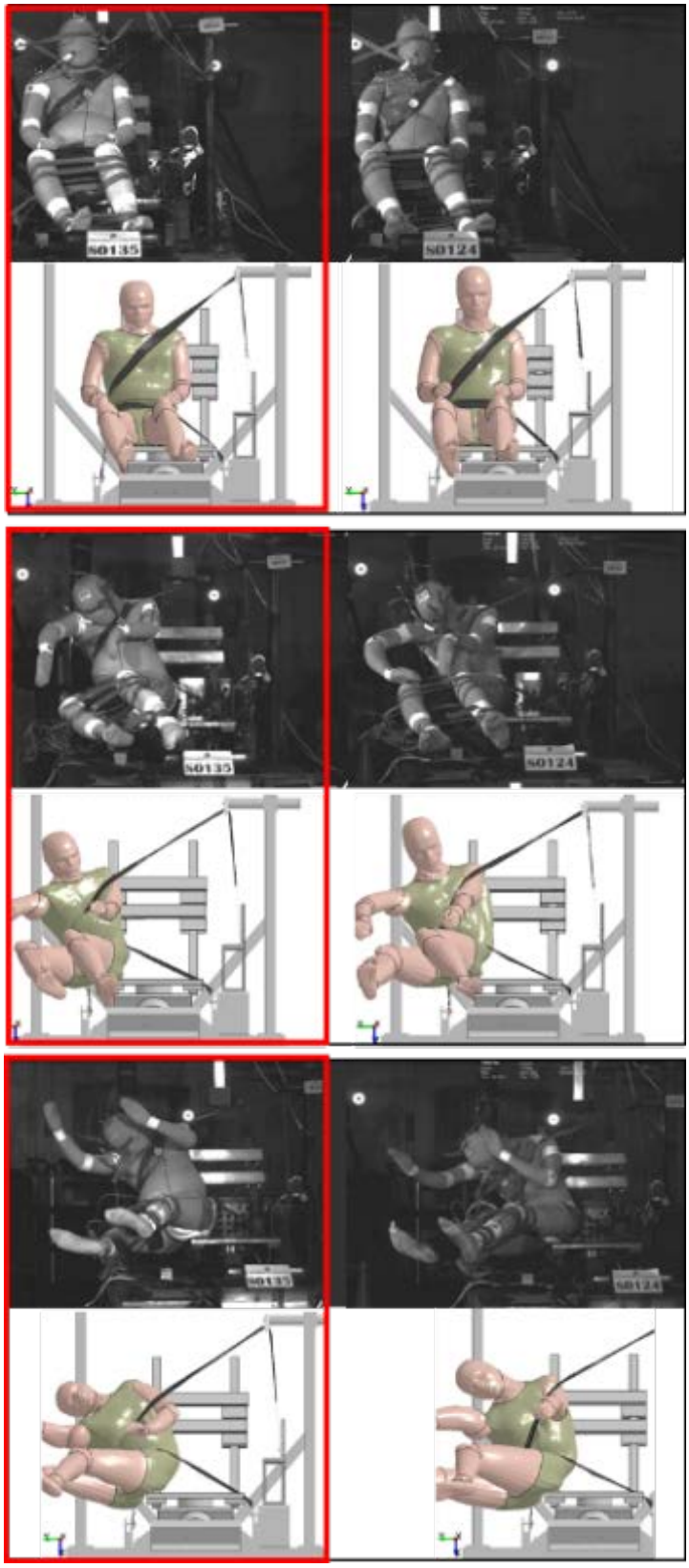

Fig. B3. Simplified GHBMC and PMHS response in Configuration 3 at 50 ms (up), 100 ms (centre) and 150 ms (down).

Fig. B4. Simplified GHBMC and PMHS response in Configuration 4 at 50 ms (up), 100 ms (centre) and 150 ms (down).

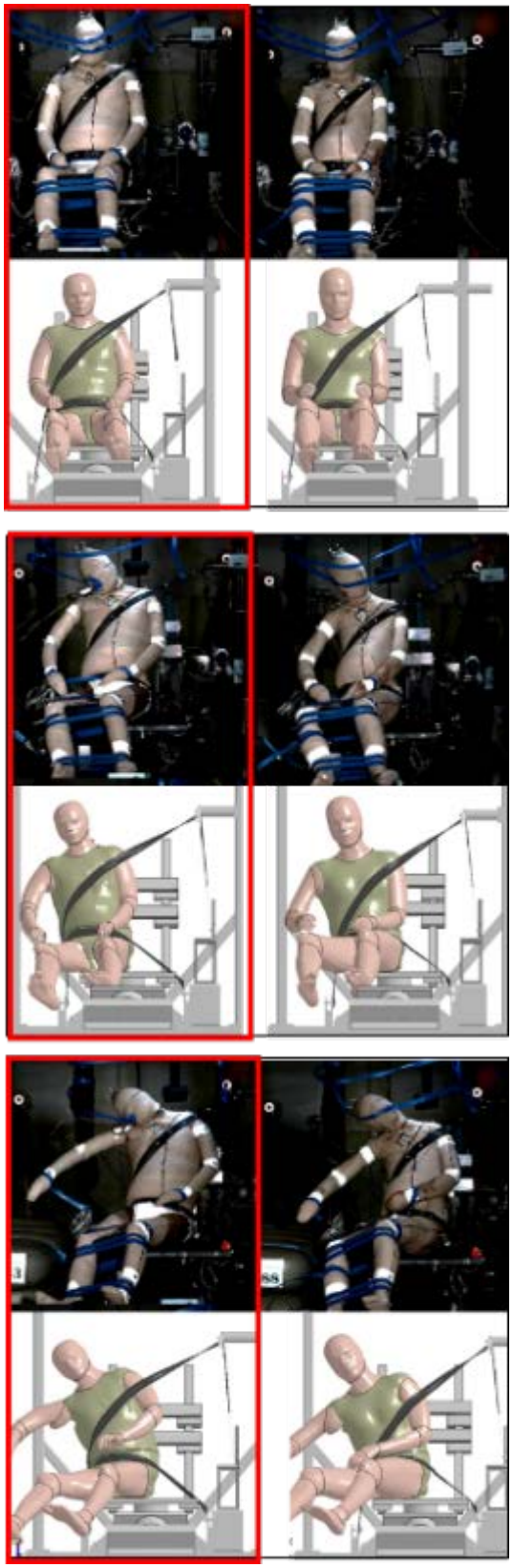

Fig. B5. Simplified GHBMC and PMHS response in Configuration 5 at 50 ms (up), 100 ms (centre) and 150 ms (down).

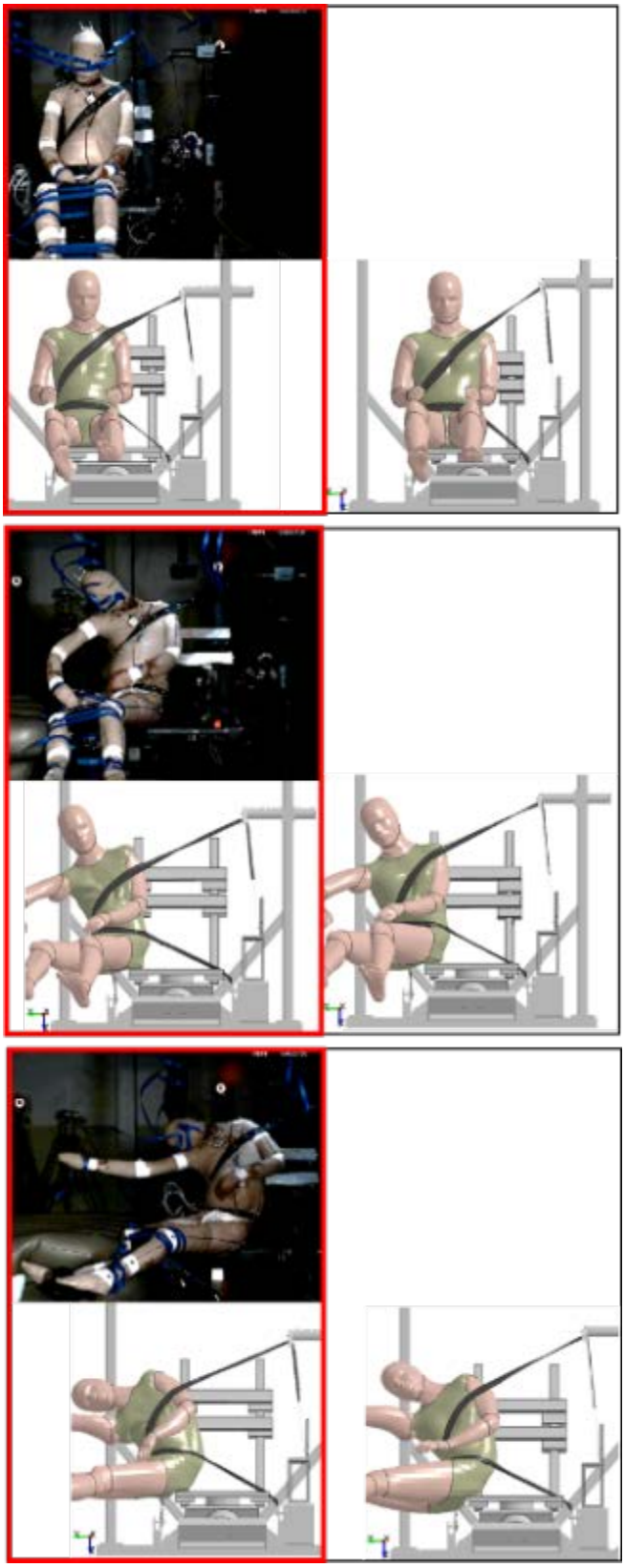

Fig. B6. Simplified GHBMC and PMHS response in Configuration 6 at 50 ms (up), 100 ms (centre) and 150 ms (down).

X. APPENDIX C

This appendix contains the CORA scores associated to head, t1 and shoulder kinematics.

TABLE C-I
EXTENDED CORA SCORES (NON-MORPHED/MORPHED)

Conf. #	Head		T1		Shoulder	Average per configuration
	Long.	Lat.	Long.	Lat.	Long.	
1	0.32 / 0.28	0.98 / 0.96	0.54 / 0.62	0.99 / 0.97	0.38 / 0.58	0.64 / 0.68
2	0.23 / 0.18	0.77 / 0.88	0.59 / 0.75	0.56 / 0.91	0.44 / 0.83	0.52 / 0.71
3	0.26 / 0.21	0.54 / 0.62	0.51 / 0.59	0.66 / 0.74	0.48 / 0.47	0.49 / 0.53
4	0.54 / 0.3	0.84 / 0.89	0.32 / 0.59	0.67 / 0.85	0.48 / 0.67	0.57 / 0.66
Average per body motion PDOF = 60°	0.34 / 0.24	0.78 / 0.84	0.49 / 0.64	0.72 / 0.87	0.45 / 0.64	0.56 / 0.64
5	0.5 / 0.69	0.66 / 0.6	0.36 / 0.65	0.54 / 0.48	0.5 / 0.61	0.51 / 0.6
6	0.96 / 0.97	0.86 / 0.67	0.78 / 0.79	0.52 / 0.48	0.83 / 0.84	0.79 / 0.75
Average per body motion PDOF = 90°	0.73 / 0.83	0.76 / 0.63	0.57 / 0.72	0.53 / 0.48	0.66 / 0.72	0.65 / 0.68
Average per body motion	0.47 / 0.44	0.78 / 0.77	0.52 / 0.67	0.66 / 0.74	0.52 / 0.67	0.59 / 0.65